Tunable Single-Ion Anisotropy in Spin-1 Models Realized with Ultracold Atoms

Woo Chang Chung, Julius de Hond, Jinggang Xiang (项晶罡), Enid Cruz-Colón, and Wolfgang Ketterle
Research Laboratory of Electronics, MIT-Harvard Center for Ultracold Atoms, Department of Physics, Massachusetts Institute of Technology, Cambridge, Massachusetts 02139, USA

(Received 4 January 2021; accepted 18 March 2021; published 23 April 2021)

Mott insulator plateaus in optical lattices are a versatile platform to study spin physics. Using sites occupied by two bosons with an internal degree of freedom, we realize a uniaxial single-ion anisotropy term proportional to $(S^z)^2$ that plays an important role in stabilizing magnetism for low-dimensional magnetic materials. Here we explore nonequilibrium spin dynamics and observe a resonant effect in the spin alignment as a function of lattice depth when exchange coupling and on-site anisotropy are similar. Our results are supported by many-body numerical simulations and are captured by the analytical solution of a two-site model.

DOI: 10.1103/PhysRevLett.126.163203

Mott insulators of ultracold atoms in optical lattices comprise a widely used platform for quantum simulations of many-body physics [1]. Since the motion of atoms is frozen out, the focus is on magnetic ordering and spin dynamics in a system with different (pseudo)spin states. As suggested in 2003, Mott insulators with two-state atoms realize quantum spin models with tunable exchange interactions and magnetic anisotropies [2,3]. Experimental achievements for spin-1/2 systems include the observation of antiferromagnetic ordering of fermions [4] and the study of spin transport in a Heisenberg spin model with tunable anisotropy of the spin-exchange couplings [5]. Spin dynamics for $S > 1$ has also been investigated [6].

However, all studies thus far have exclusively addressed spin systems with occupations of one atom per site. This limits spin Hamiltonians to spin-exchange terms between different sites i, j proportional to $\sum_{\langle ij\rangle} S_i^k S_j^k$ (where $k \in \{x, y, z\}$) and to Zeeman couplings to effective magnetic fields, proportional to $\sum_i S_i^z$. For Mott insulators with two or more atoms per site, the Hubbard model has direct on-site interactions that can give rise to a nonlinear term $D\sum_i (S_i^z)^2$, where D is the so-called single-ion anisotropy constant. $(S^z)^2$ terms, which are present for $S \geq 1$ only, are important for establishing nontrivial correlations such as in spin squeezing [7]. In spin-1 models, such terms can lead to a qualitatively new magnetic phase diagram [8,9]. For example, for ferromagnetic spin-1 Heisenberg models, the single-ion anisotropy gives rise to a gapped spin state (the "spin Mott insulator") that can be used as an initial low-entropy state for an adiabatic ramp toward a highly correlated gapless spin state (the XY ferromagnet) [10,11]. For antiferromagnetic systems in one dimension, the single-ion anisotropy leads to a quantum phase transition between a topologically trivial phase and a nontrivial phase as predicted by Haldane [12–14]. The magnetic properties of many materials crucially depend on crystal field anisotropies that break rotational symmetry and can stabilize ferromagnetism in two-dimensional materials by avoiding the Mermin-Wagner theorem, which forbids long-range order for continuous symmetries [15,16]. The interest in spin-1 systems is demonstrated by various studies on different platforms [17–19].

In this Letter, we use cold atoms in optical lattices to implement a spin-1 Heisenberg Hamiltonian using a Mott insulator of doubly occupied sites and demonstrate dynamical features that arise from the single-ion anisotropy. For spin-exchange interactions studied thus far in optical lattices, the only timescale for dynamics is second-order tunneling (i.e., superexchange), which monotonically slows down for deeper lattices. In contrast, as we show here, the single-ion anisotropy introduces a new timescale, and we find a dynamical behavior that is faster in deeper lattices due to a resonance effect when the energies of superexchange and single-ion anisotropy are comparable.

We present a protocol to directly measure the anisotropy in the spin distribution and find a pronounced transient behavior of this quantity when the resonance condition is met. Transients change sign along with the single-ion anisotropy. We find good agreement with theoretical simulations and explain the most salient features using a two-site model with an exact solution.

In the Mott insulator regime, the optical lattices are sufficiently deep that the on-site interaction suppresses first-order tunneling, and exchange processes are only possible via second-order tunneling. For two atoms per site with two internal states, the Bose-Hubbard Hamiltonian is approximated by an effective spin Hamiltonian

$$H = -J\sum_{\langle ij\rangle} \mathbf{S}_i \cdot \mathbf{S}_j + D\sum_i (S_i^z)^2 - B\sum_i S_i^z, \qquad (1)$$

where $\mathbf{S}_i$ are spin-1 operators, $\langle ij \rangle$ are pairs of nearest-neighboring sites, J is the exchange constant, D is the uniaxial single-ion anisotropy constant, and B is a fictitious magnetic bias field. The spin-1 operators are related to the boson creation and annihilation operators via $S_i^z = (a_i^\dagger a_i - b_i^\dagger b_i)/2$, $S_i^+ = a_i^\dagger b_i$, $S_i^- = b_i^\dagger a_i$ under the constraint $a_i^\dagger a_i + b_i^\dagger b_i = 2$, where a_i and b_i are boson annihilation operators at site i for state a and state b, respectively. In terms of the tunneling amplitude t and interaction energies $U_{\sigma\sigma'}$: $J = 4t^2/U_{ab}$ and $D = (U_{aa} + U_{bb})/2 - U_{ab}$, where $U_{\sigma\sigma'}$ represents the on-site interaction energy between atoms in two states $\sigma, \sigma' \in \{a, b\}$. The term proportional to B can be dropped if the total longitudinal magnetization $\sum_i S_i^z$ is constant, as it is in the experiment.

For the species studied here, ^{87}Rb, all $U_{\sigma\sigma'}$ differ by less than 1%, and therefore all spin-exchange couplings are almost equal, resulting in isotropic spin Hamiltonians for site occupancy $\nu = 1$. However, for $\nu = 2$, we can tune the relevant anisotropy parameter D/J over a large range of values because J decreases exponentially with lattice depth while D—a differential on-site energy—slowly increases.

The experimental sequence begins by preparing a Bose-Einstein condensate (BEC) of ^{87}Rb atoms in the $|F = 1, m_F = -1\rangle$ hyperfine state inside a crossed optical dipole trap. The sequence proceeds by loading the BEC into a deep three-dimensional optical lattice formed by retroreflected lasers with wavelengths of $\lambda = 1064$ nm. The lattices are ramped to final depths of $30E_R$ in 250 ms, where $E_R = h^2/(2m\lambda^2)$ is the recoil energy for atomic mass m. Experimental parameters are chosen to maximize the size of the $\nu = 2$ Mott-insulator plateau without significant population of sites with $\nu = 3$ [see Fig. 1(a) and Ref. [20]].

To allow for spin dynamics, all atoms are rotated into an equal superposition of two hyperfine states $(|a\rangle - i|b\rangle)/\sqrt{2}$ using a combination of microwave pulses [20]. This initial state is a simple product state. Negative and positive values of D are realized with the pairs $|a\rangle = |1, -1\rangle$, $|b\rangle = |1, 1\rangle$ and $|a\rangle = |1, -1\rangle$, $|b\rangle = |1, 0\rangle$, respectively [20]. The spin-exchange dynamics in one-dimensional chains is initiated by a 3-ms quench, during which we ramp down the longitudinal lattice to a variable depth while the transverse lattices are ramped up to $35E_R$ [Fig. 1(b)]. After a variable evolution time, the final spin configuration is "frozen in" by ramping the longitudinal lattice to $35E_R$ as well [Fig. 1(c)].

Our observable for the anisotropy in the spin distribution is the longitudinal spin alignment $A = S(S+1) - 3\langle (S^z)^2 \rangle$, measured in the $\nu = 2$ plateau. $\langle (S^z)^2 \rangle = \sum_{i=1}^N \langle (S_i^z)^2 \rangle / N$ is the average on-site longitudinal spin correlation. A is defined to be zero for a random distribution of spins. Since $S^z = 1, 0, -1$ for the $|aa\rangle$, $|ab\rangle$, and $|bb\rangle$ doublons, respectively, A can be obtained by measuring the relative abundance of the different doublons. Specifically, we refer to the fraction of $|ab\rangle$ doublons as the "spin-paired doublon fraction" f.

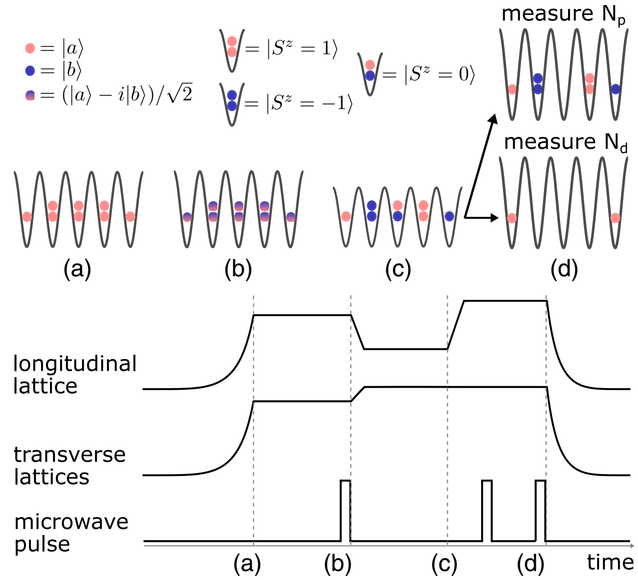

FIG. 1. Experimental sequence for the measurement of spin alignment and doublon fractions. (a) The lattices are ramped up to initialize a single-component Mott insulator with a maximal site occupancy of two. (b) Microwave pulses prepare a superposition of two hyperfine states $(|a\rangle - i|b\rangle)/\sqrt{2}$. Ramping down the longitudinal lattice initiates spin-exchange dynamics. (c) Ramping up the lattices stops the exchange dynamics. Microwave pulses transfer the two components to a pair of states with a Feshbach resonance. (d) Either $|ab\rangle$ doublons or all doublons are removed with the help of Feshbach-enhanced inelastic losses. The remaining atoms are transferred back to the $F = 1$ hyperfine states and are counted via absorption imaging to measure N_p or N_d.

Since $\langle (S^z)^2 \rangle = 1 - f$, we obtain $A = 3f - 1$. The doublon statistics can be measured by selectively introducing a fast loss process that targets a specific type of doublon and by comparing the remaining total numbers of atoms, which are measured via absorption imaging. Specifically, if N_a is the average total atom number in the whole cloud, N_p the average number of remaining atoms after removing $|ab\rangle$ doublons, and N_d the average number of remaining atoms after removing all doublons, then $f = (N_a - N_p)/(N_a - N_d)$ [Fig. 1(d)]. Fast losses of doublons are induced by transferring the atoms to hyperfine states for which inelastic two-body loss is enhanced near two narrow Feshbach resonances around a magnetic field of 9 G [20,28]. Since f and A are obtained from the ratio of differences in atom numbers, good atom number stability in the experiment (the deviation from mean being typically $< 4\%$) was crucial to measure A with sufficiently small uncertainties.

For the initial state, $f = 1/2$ and $A = 1/2$. Over times that are long compared to the spin-exchange timescale $\hbar/J$, heating processes drive the system toward thermal equilibrium with $A = 0$. At short times, coherent spin dynamics is observed: If D is negative, the $|aa\rangle$ and $|bb\rangle$ doublons are energetically favorable, and we expect f and A to decrease. If D is positive, the $|ab\rangle$ doublons are favorable, and we expect f and A to increase. If D is zero, the system is described by an isotropic spin-1 Heisenberg Hamiltonian of which the initial state is an eigenstate. By fixing the hold time and scanning the value of the lattice depth for the spin chains, we can monitor the impact of D/J on the dynamical change in A. For positive (negative) D, we chose a hold time of 70 ms (25 ms). These hold times are chosen to be comparable to $\hbar/J$ when $|D/J| \sim 1$ [20].

Figure 2 shows that for $|D/J| \ll 1$ or $|D/J| \gg 1$, A stays near its initial value of 1/2. However, when $D/J \sim 2$, which corresponds to a longitudinal lattice depth of $14E_R$ ($11E_R$) for positive D (negative D), we see that A reaches a maximum (minimum). This nonmonotonic change of A with lattice depth is indicative of the interplay between spin-exchange and single-ion anisotropy. In addition, we observe that the change in A is smaller for positive D than for negative D.

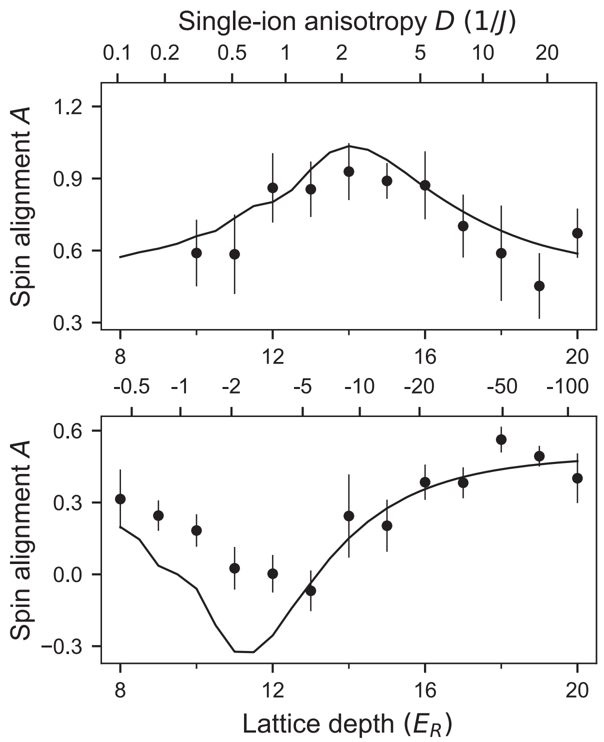

FIG. 2. Transient enhancement and reduction of the spin alignment A by coherent spin dynamics. The change in A is strongest when $|D/J| \sim 2$. Measurements were done for both positive (top) and negative (bottom) values of D/J. The atoms were held for 70 ms and 25 ms, respectively (also see Fig. 4). The top axis in both figures indicates the D/J ratio. Solid lines are the results of matrix-product state–time-evolving block decimation (MPS-TEBD) calculations. The error bars represent the standard error of the mean for A, obtained by error propagation after averaging three measurements for each of N_a, N_p, and N_d. We found the error bars to be dominated by fluctuations in prepared atom number over systematic errors. For the lowest lattice depths, the spin model may not fully represent the Bose-Hubbard model.

Several aspects of the observed spin dynamics can be captured by a two-site model. Although states on two spin-1 sites span a 9-dimensional Hilbert space, we can reduce the spin dynamics to a beat note between two states. Since exchange interactions do not change the total magnetization $\sum_{i=1}^{N} S_i^z$, the Hilbert space factorizes to subspaces with the same total magnetization (although S_i^z can differ within a subspace). Furthermore, the initial superposition state is symmetric between the left and right wells, and any change in A comes from the two coupled states: $|ab\rangle_L|ab\rangle_R$ and $(|aa\rangle_L|bb\rangle_R + |bb\rangle_L|aa\rangle_R)/\sqrt{2}$, for which A equals 2 and -1, respectively (Fig. 3). By describing these two states as two poles on a Bloch sphere, we see that the initial state is represented by a vector pointing somewhere between the north pole and the equator with a vertical fictitious external field. The quench in J and D suddenly changes the strength and the orientation of this external field and induces a precession of the state vector around the new external field [20]. This results in an oscillation of A with amplitude

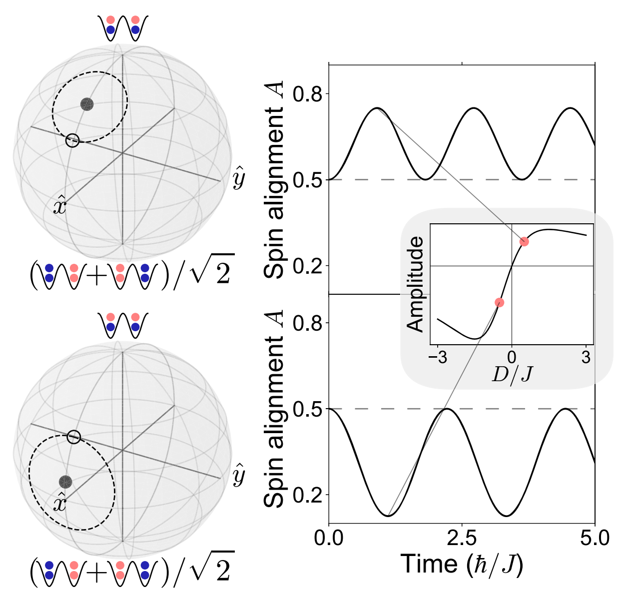

FIG. 3. Coherent spin oscillations in a two-site model. While the full basis contains nine states, the oscillations in the spin alignment A involve only a 2×2 block of the Hamiltonian. This allows us to illustrate the dynamics on Bloch spheres (left), where the initial state is represented by the open circle. If $J = 0$, the effective magnetic field points along $\hat{z}$, and the purely azimuthal precession will not change A. If $J > 0$, the effective magnetic field is tilted, resulting in a precession along the dashed circle, which is observed as an oscillation in A (right). The frequency of the oscillation, in units of $J/\hbar$, is given by $\Omega = \sqrt{9 + 4D/J + 4(D/J)^2}$, and its peak-to-peak amplitude is $6(D/J)/[9 + 4D/J + 4(D/J)^2]$ (see inset). This shows that the direction of oscillation depends on the sign of D/J (compare top and bottom rows, where $D/J = 0.5$ and -0.5, respectively). Note that while the initial value of A for this subspace is 1, the contribution of other states sets the initial A of the whole system to 1/2.

$6(D/J)/[9 + 4D/J + 4(D/J)^2]$. This function has local extrema for $D/J = \pm 3/2$ but is not symmetric around $D/J = 0$. This explains the nonmonotonic behavior as a function of lattice depth and shows why the contrast is smaller for positive D/J than for negative D/J.

One would expect that, for a larger number of sites, additional precession frequencies appear, turning the periodic oscillation for two sites into a relaxation toward an asymptotic value, which, according to the eigenstate thermalization hypothesis, represents a low-temperature equilibrium [29]. Comparison between the two-site model and a many-site model numerically simulated using the time-evolving block decimation for matrix-product states (MPS-TEBD) shows that the initial change in A is indeed well captured by the two-site model [20]. Because of the spin dynamics, the system evolves from a product state into a highly correlated state with entanglement between sites; this has been the focus of recent theoretical works [30,31]. In the two-site model, the von Neumann entanglement entropy can reach up to $\sim 0.9 \times \ln(3)$ due to the interplay between single-ion anisotropy and exchange terms. This corresponds to an almost maximally entangled state since $\ln(3)$ is the maximum entropy for a spin-1 site.

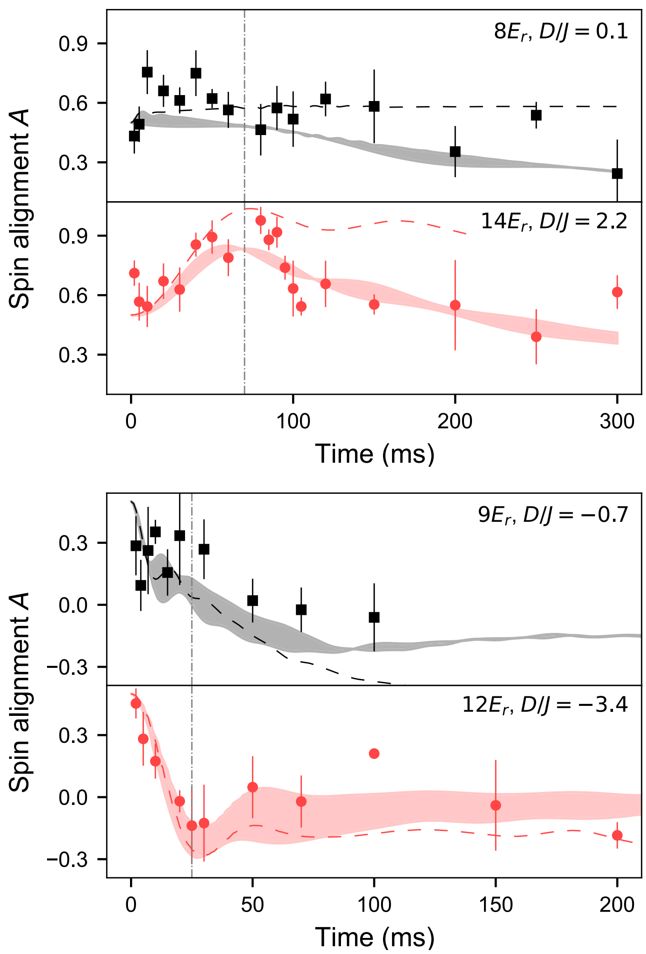

FIG. 4. Coherent dynamics of the spin alignment A after a quench in D/J. Varying the hold time at characteristic lattice depths for both positive and negative values of D/J (top and bottom pairs of panels, respectively) reveals that strong transients in A only occur at intermediate lattice depth for which D and J are comparable. The vertical dash-dotted lines indicate the hold times used for these pairs in Fig. 2. Dashed lines are the results of the MPS-TEBD simulation. The shaded regions denote the MPS-TEBD results with $\pm 0.5 E_R$ uncertainty in the lattice depths and include exponential decay toward a thermal spin state with $A = 0$ with empirical $1/e$ times of 350 ms ($D > 0$) and 175 ms ($D < 0$), the ratio of which reflects the relative sensitivity to ambient magnetic field fluctuations of the pairs. The error bars are computed in the same manner as those in Fig. 2.

To show that changes in the spin alignment A result from competition between the exchange interaction and the single-ion anisotropy, we study the time evolution of A at two different lattice depths (Fig. 4). For positive D, MPS-TEBD simulations predict very little change in A at a lower lattice depth, where the exchange constant is relatively large, but the anisotropy is small, while it predicts a noticeable change in A at a higher lattice depth, where the exchange constant and the anisotropy term become comparable. While the simulation predicts equilibration of A to an asymptotic value (thin lines), measurements show that it decays toward a lower value for positive D and does not decrease as much as the simulation predicts for negative D. The measurements are consistent with the fact that at high spin temperatures, the spin distribution becomes isotropic and A vanishes. Indeed, when we ramp down the lattices and retrieve a BEC, we observe a significant reduction of the condensate fraction after 300 ms. This represents the timescale over which entropy is either transported through the cloud or created by heating. It could possibly be extended by better stabilizing ambient field fluctuations or by adding a tilt to suppress entropy transport by holes [32].

In conclusion, we have implemented a spin-1 Heisenberg model with a single-ion anisotropy using the $\nu = 2$ plateau of a Mott insulator and have observed the subtle interplay between spin-exchange and on-site anisotropy in coherent spin dynamics. Much larger values of D can be implemented with spin-dependent lattices, which will allow us to observe much faster anisotropy-driven dynamics and will also enable mapping out the phase diagram of the anisotropic spin Hamiltonian [11]. It should also be noted that it is possible to change the sign of J with the gradient of an optical dipole potential [32,33], which will permit exploration of the antiferromagnetic sector with bosons. Interesting dynamical features of anisotropic spin models have been predicted [34], including transient spin currents, implying counterflow superfluidity.

Regarding quantum simulations, single-ion anisotropies play a crucial role in magnetic materials (e.g., monolayers containing chromium [35,36]). In such materials, crystal field effects lift the degeneracy of d orbitals, and spin-orbit interaction transfers this anisotropy to the electronic spins responsible for the magnetism [37]. Here we have simulated this anisotropy by selecting a pair of atomic hyperfine states where the interspecies scattering length is different from the average of the intraspecies values. This illustrates the potential for ultracold atoms in optical lattices to implement idealized Hamiltonians describing important materials.

We thank Colin Kennedy, William Cody Burton, and Wenlan Chen for contributions to the development of experimental techniques and Ivana Dimitrova and Andrew Daley for their critical reading of the manuscript. We acknowledge support from the NSF through the Center for Ultracold Atoms and Grant No. 1506369, ARO-MURI Non-equilibrium Many-Body Dynamics (Grant No. W911NF14-1-0003), AFOSR-MURI Quantum Phases of Matter (Grant No. FA9550-14-1-0035), ONR (Grant No. N00014-17-1-2253), and a Vannevar-Bush Faculty Fellowship. W. C. C. acknowledges additional support from the Samsung Scholarship.

W. C. C. and J. d.-H. contributed equally to this work.

[1] I. Bloch, J. Dalibard, and W. Zwerger, Rev. Mod. Phys. **80**, 885 (2008).
[2] L.-M. Duan, E. Demler, and M. D. Lukin, Phys. Rev. Lett. **91**, 090402 (2003).
[3] A. B. Kuklov and B. V. Svistunov, Phys. Rev. Lett. **90**, 100401 (2003).
[4] A. Mazurenko, C. S. Chiu, G. Ji, M. F. Parsons, M. Kanász-Nagy, R. Schmidt, F. Grusdt, E. Demler, D. Greiff, and M. Greiner, Nature (London) **545**, 462 (2017).
[5] P. N. Jepsen, J. Amato-Grill, I. Dimitrova, W. W. Ho, E. Demler, and W. Ketterle, Nature (London) **588**, 403 (2020).
[6] A. de Paz, A. Sharma, A. Chotia, E. Maréchal, J. H. Huckans, P. Pedri, L. Santos, O. Gorceix, L. Vernac, and B. Laburthe-Tolra, Phys. Rev. Lett. **111**, 185305 (2013).
[7] M. Kitagawa and M. Ueda, Phys. Rev. A **47**, 5138 (1993).
[8] Y. Li, M. R. Bakhtiari, L. He, and W. Hofstetter, Phys. Rev. B **84**, 144411 (2011).
[9] Y. Li, L. He, and W. Hofstetter, Phys. Rev. A **93**, 033622 (2016).
[10] E. Altman, W. Hofstetter, E. Demler, and M. D. Lukin, New J. Phys. **5**, 113 (2003).
[11] J. Schachenmayer, D. M. Weld, H. Miyake, G. A. Siviloglou, W. Ketterle, and A. J. Daley, Phys. Rev. A **92**, 041602(R) (2015).
[12] F. D. M. Haldane, Phys. Lett. **93A**, 464 (1983).
[13] F. D. M. Haldane, Phys. Rev. Lett. **50**, 1153 (1983).
[14] F. D. M. Haldane, Rev. Mod. Phys. **89**, 040502 (2017).
[15] N. D. Mermin and H. Wagner, Phys. Rev. Lett. **17**, 1133 (1966).
[16] J. Strečka, D. Ján, and L. Čanová, Chin. J. Phys. **46**, 329 (2008), https://www.ps-taiwan.org/cjp/issues.php?vol=46#=3.
[17] J. P. Renard, M. Verdaguer, L. P. Regnault, W. A. C. Erkelens, J. Rossat-Mignod, and W. G. Stirling, Europhys. Lett. **3**, 945 (1987).
[18] P. Chauhan, F. Mahmood, H. J. Changlani, S. M. Koohpayeh, and N. P. Armitage, Phys. Rev. Lett. **124**, 037203 (2020).
[19] C. Senko, P. Richerme, J. Smith, A. Lee, I. Cohen, A. Retzker, and C. Monroe, Phys. Rev. X **5**, 021026 (2015).
[20] See Supplemental Material at http://link.aps.org/supplemental/10.1103/PhysRevLett.126.163203 for the calculation of D and J values, the confinement parameters, the details of state preparation and doublon measurement, the derivation of the two-site model, and a description of our matrix-product state simulations, with Refs. [21–27] therein.
[21] N. Marzari and D. Vanderbilt, Phys. Rev. B **56**, 12847 (1997).
[22] W. Kohn, Phys. Rev. **115**, 809 (1959).
[23] P. Cheinet, S. Trotzky, M. Feld, U. Schnorrberger, M. Moreno-Cardoner, S. Fölling, and I. Bloch, Phys. Rev. Lett. **101**, 090404 (2008).
[24] G. K. Campbell, J. Mun, M. Boyd, P. Medley, A. E. Leanhardt, L. G. Marcassa, D. E. Pritchard, and W. Ketterle, Science **313**, 649 (2006).
[25] D. M. Stamper-Kurn and M. Ueda, Rev. Mod. Phys. **85**, 1191 (2013).
[26] J. Hauschild and F. Pollmann, SciPost Phys. Lect. Notes 5 (2018).
[27] G. Vidal, Phys. Rev. Lett. **93**, 040502 (2004).
[28] A. M. Kaufman, R. P. Anderson, T. M. Hanna, E. Tiesinga, P. S. Julienne, and D. S. Hall, Phys. Rev. A **80**, 050701(R) (2009).
[29] J. M. Deutsch, Rep. Prog. Phys. **81**, 082001 (2018).
[30] I. Morera, A. Polls, and B. Juliá-Díaz, Sci. Rep. **9**, 9424 (2019).
[31] A. Venegas-Gomez, J. Schachenmayer, A. S. Buyskikh, W. Ketterle, M. L. Chiofalo, and A. J. Daley, Quantum Sci. Technol. **5**, 045013 (2020).
[32] I. Dimitrova, N. Jepsen, A. Buyskikh, A. Venegas-Gomez, J. Amato-Grill, A. Daley, and W. Ketterle, Phys. Rev. Lett. **124**, 043204 (2020).
[33] H. Sun, B. Yang, H.-Y. Wang, Z.-Y. Zhou, G.-X. Su, H.-N. Dai, Z.-S. Yuan, and J.-W. Pan, arXiv:2009.01426.
[34] A. Venegas-Gomez, A. S. Buyskikh, J. Schachenmayer, W. Ketterle, and A. J. Daley, Phys. Rev. A **102**, 023321 (2020).
[35] C. Gong, L. Li, Z. Li, H. Ji, A. Stern, Y. Xia, T. Cao, W. Bao, C. Wang, Y. Wang *et al.*, Nature (London) **546**, 265 (2017).
[36] C. Xu, J. Feng, H. Xiang, and L. Bellaiche, npj Comput. Mater. **4**, 57 (2018).
[37] D. Dai, H. Xiang, and M.-H. Whangbo, J. Comput. Chem. **29**, 2187 (2008).